THE JOURNAL OF PHYSICAL CHEMISTRY A

Article

pubs.acs.org/JPCA

Infrared Absorption of Gaseous Benzoyl Radical C_6H_5CO Recorded with a Step-Scan Fourier-Transform Spectrometer

Shu-Yu Lin[†] and Yuan-Pern Lee*[,†,‡]

[†]Department of Applied Chemistry and Institute of Molecular Science, National Chiao Tung University, Hsinchu 30010, Taiwan

[‡]Institute of Atomic and Molecular Sciences, Academia Sinica, Taipei 10617, Taiwan

Supporting Information

ABSTRACT: A step-scan Fourier-transform infrared spectrometer coupled with a multipass absorption cell was utilized to monitor the gaseous transient species benzoyl radical, C_6H_5CO. C_6H_5CO was produced either from photolysis of acetophenone, $C_6H_5C(O)CH_3$, at 248 nm or in reactions of phenyl radical (C_6H_5) with CO; C_6H_5 was produced on photolysis of C_6H_5Br at 248 nm. One intense band at 1838 ± 1 cm^{-1}, one weak band at 1131 ± 3 cm^{-1}, and two extremely weak bands at 1438 ± 5 and 1590 ± 10 cm^{-1} are assigned to the C═O stretching (ν_6), the C−C stretching mixed with C−H deformation (ν_{15}), the out-of-phase $C_1C_2C_3/C_5C_6C_1$ symmetric stretching (ν_{10}), and the in-phase $C_1C_2C_3/C_4C_5C_6$ antisymmetric stretching (ν_7) modes of C_6H_5CO, respectively. These observed vibrational wavenumbers and relative IR intensities agree with those reported for C_6H_5CO isolated in solid Ar and with values predicted for C_6H_5CO with the B3LYP/aug-cc-pVDZ method. The rotational contours of the two bands near 1838 and 1131 cm^{-1} simulated according to rotational parameters predicted with the B3LYP/aug-cc-pVDZ method fit satisfactorily with the experimental results. Additional products BrCO, $C_6H_5C(O)Br$, and $C_6H_5C(O)C_6H_5$ were identified in the $C_6H_5Br/CO/N_2$ experiments; the kinetics involving C_6H_5CO and $C_6H_5C(O)Br$ are discussed.

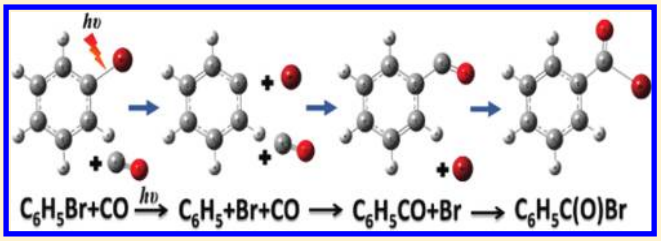

INTRODUCTION

The benzoyl (C_6H_5CO) radical, which is produced in the combustion of aromatic hydrocarbons from the reaction of C_6H_5 with CO[1] or in the atmosphere as a result of the reaction of C_6H_5CHO with OH, Cl, or NO_3,[2,3] readily reacts with oxygen in these systems to form benzoylperoxy radical, $C_6H_5C(O)OO$.[4] $C_6H_5C(O)OO$ is a precursor of the air pollutant peroxybenzoyl nitrate, $C_6H_5C(O)O_2NO_2$, a lachrymator[5] that has been detected in the photochemical smog.[6] C_6H_5CO has also been identified as an important intermediate in the formation of polycyclic aromatic hydrocarbons (PAH), which lead to soot formation.[7] In industry, C_6H_5CO is an important intermediate produced on photoirradiation of aryl ketones to initiate polymerization.[8,9]

C_6H_5CO in a solution of 3-methyl-3-pentanol has an ultraviolet (UV) absorption band with maximal cross-section of 2.5 × 10^{-22} cm^2 $molecule^{-1}$ at 368 nm and a weaker broad band near 480 nm.[10] Bennett and Mile produced C_6H_5CO from a reaction of $C_6H_5C(O)Cl$ + Na, trapped it in various matrixes for electron paramagnetic resonance spectroscopy, and reported that C_6H_5CO is a σ-type radical with the unpaired electron localized in the sp hybrid orbital of the C═O moiety; the C−C═O bond angle was estimated to be 130°.[11] Reported kinetic experiments of C_6H_5CO employed only mass spectrometry to monitor this radical.[4]

The infrared (IR) spectrum of C_6H_5CO in solutions was investigated with time-resolved IR spectroscopy, but only the C═O stretching band of C_6H_5CO near 1828 cm^{-1} (in hexane),[12] 1818 cm^{-1} (in acetonitrile),[13] or 1824 cm^{-1} (in CCl_4)[14] was observed. Mardyukov and Sander produced C_6H_5CO on reacting phenyl radicals with CO before deposition into an Ar matrix and characterized it with IR spectroscopy; their reported vibrational wavenumbers agree satisfactorily with those predicted with the UB3LYP/cc-pVTZ method.[15] The IR spectrum of C_6H_5CO in the gaseous phase is unreported.

We have recorded IR spectra of several gaseous reaction intermediates using a step-scan Fourier-transform spectrometer coupled with a multipass absorption cell.[16−18] With this method, we identified IR absorption band origins at 1830, 1226, 1187, and 1108 cm^{-1} of *syn*-$C_6H_5C(O)OO$ in the reaction of C_6H_5CO with O_2.[19] Here, we report an extension of that work to characterize the IR absorption spectra of gaseous C_6H_5CO radicals with a step-scan IR spectrometer.

EXPERIMENTS AND COMPUTATIONS

The experimental setup has been described previously;[20] only a brief description is given here. A step-scan Fourier-transform infrared spectrometer (FTIR, Thermo Nicolet, Nexus 870) coupled with a multireflection White cell was employed to

Special Issue: A. R. Ravishankara Festschrift

Received: December 15, 2011
Revised: February 26, 2012
Published: February 27, 2012

   dx.doi.org/10.1021/jp2120934 | J. Phys. Chem. A 2012, 116, 6366−6374

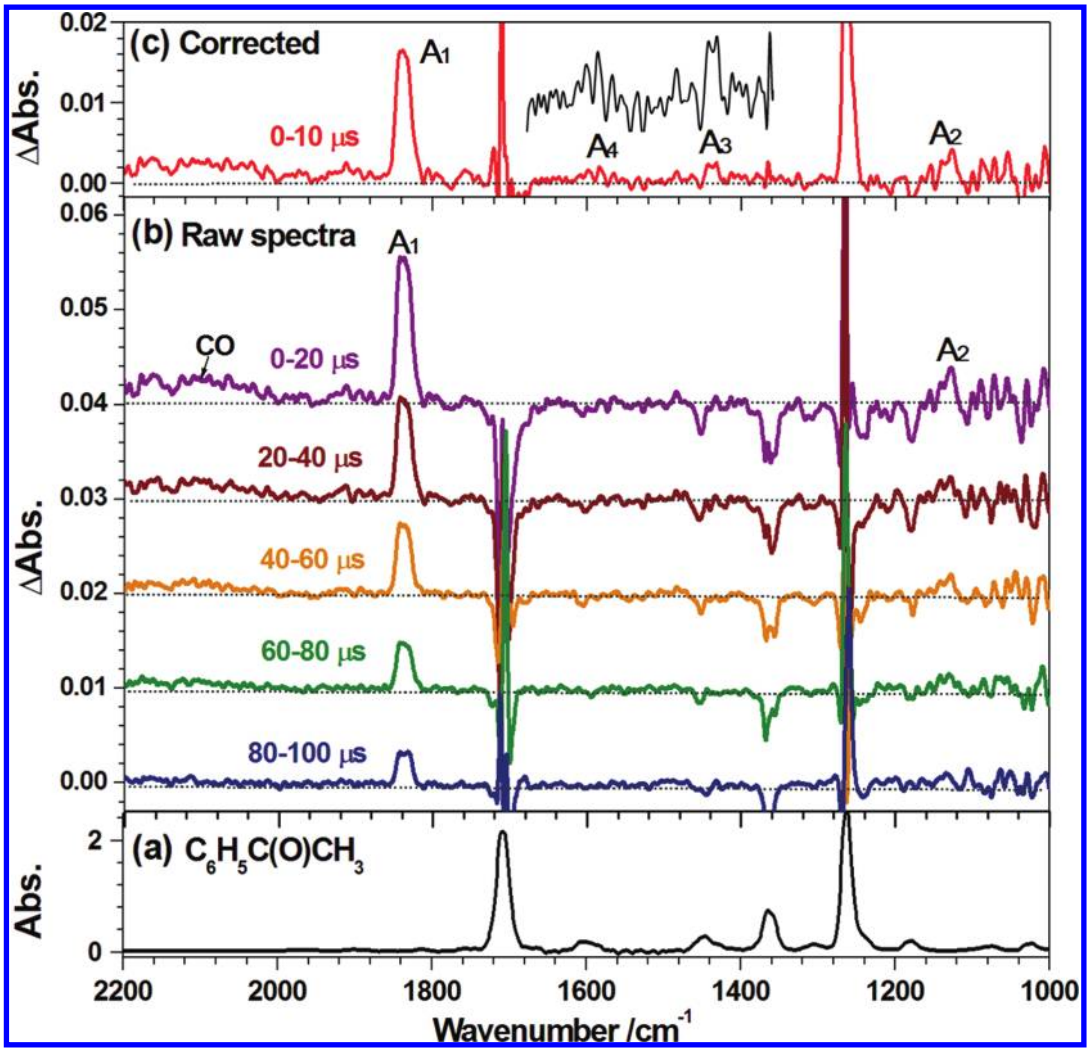

Figure 1. (a) Absorption of $C_6H_5C(O)CH_3$ in the region 2200−1000 cm^{-1}. (b) Transient difference absorption spectra at 20 μs intervals upon laser photolysis at 248 nm (5 Hz, 43 mJ cm^{-2}) of a flowing mixture of $C_6H_5C(O)CH_3/N_2$ (1/213) at 107 Torr and 363 K; resolution is 4 cm^{-1}. (c) Absorption spectrum integrated for 0−10 μs and corrected for the loss of $C_6H_5C(O)CH_3$; see text.

record the IR spectra of transient species. The White cell with a base path length of 20 cm and effective path length of 6.4 m was placed in the sample compartment of the FTIR and served as a flow reactor. The flow reactor has a volume of ∼1600 cm^3 and accommodates two rectangular quartz windows (3 × 12 cm^2) on opposite sides of the cell to allow the photolysis beam to propagate approximately perpendicularly to the multiply passed IR beam. The laser beam, of wavelength 248 nm generated from a KrF excimer laser (Lambda Physik, LPX240i, 5 Hz, 86−92 mJ $pulse^{-1}$, beam size 2 × 1 cm^2), passed these quartz windows and was reflected once with an external laser mirror to photodissociate a flowing mixture of $C_6H_5C(O)CH_3$ in N_2 or C_6H_5Br and CO in N_2.

The IR probing light was detected with a HgCdTe detector (preamplifier bandwidth 20 MHz) from which dc- and ac-coupled signals were recorded at each scan step upon irradiation with the photolysis laser. The dc-coupled signal was sent directly to the internal 16-bit digitizer (2 × 10^5 samples s^{-1}) of the spectrometer, whereas the ac-coupled signal was amplified 20 times before being transferred to a fast external 14-bit digitizer (10^8 samples s^{-1}). These signals were typically averaged over 10 laser shots at each scan step. For the ac signal, 300 data points at 1 μs integrated intervals were acquired to cover a period of 300 μs after photolysis. With appropriate optical filters to define a narrow spectral region, we performed under-sampling to decrease the size of the interferogram, hence the duration of data acquisition. For spectra in the range 800−2500 cm^{-1} at resolution of 4 cm^{-1}, 1528 scan steps were completed within 3 h. For spectra in the range 1600−2035 cm^{-1} at resolution of 2 cm^{-1}, 424 scan steps were completed within 40 min. After completion of all scan steps, the data were sorted to produce interferograms corresponding to each time interval. The derivation of conventional time-resolved difference absorption spectra from these data has been established previously.[20,21]

For experiments with $C_6H_5C(O)CH_3/N_2$, a small stream of N_2 from a main stream at flow rate of $F_{N2} \cong 23$ STP cm^3 s^{-1} (STP donates standard temperature 273.15 K and pressure 1 atm) was bubbled through $C_6H_5C(O)CH_3$. The total pressure was maintained in the range P_T = 100−110 Torr with a partial pressure $P_{C6H5C(O)CH3} \cong 0.5$ Torr of acetophenone determined from its IR absorption spectra. The efficiency of photolysis of $C_6H_5C(O)CH_3$ is estimated to be ∼80% according to an absorption cross-section of ∼2.9 × 10^{-17} cm^2 $molecule^{-1}$ (ref 22) and a laser fluence of ∼5.4 × 10^{16} photons cm^{-2} at 248 nm.

dx.doi.org/10.1021/jp2120934 | J. Phys. Chem. A 2012, 116, 6366−6374

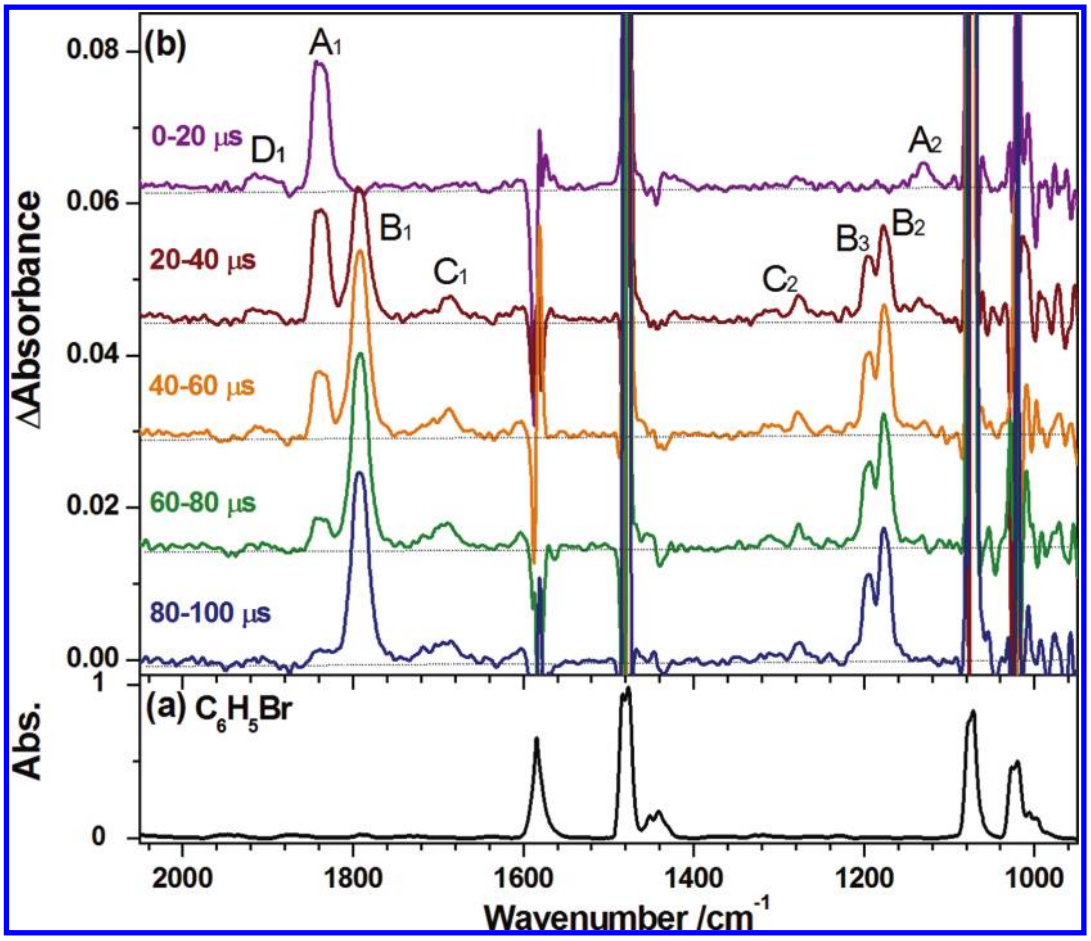

Figure 2. (a) Absorption of C_6H_5Br in the region 2050−950 cm^{-1}. (b) Transient difference absorption spectra at 20 μs intervals upon laser photolysis at 248 nm (5 Hz, 46 mJ cm^{-2}) of a flowing mixture of $C_6H_5Br/CO/N_2$ (1/47/42) at 134 Torr and 363 K; resolution is 4 cm^{-1}.

For experiments with $C_6H_5Br/CO/N_2$, a small stream of N_2 from the main stream was bubbled through C_6H_5Br. The flow rates of CO and N_2 were $F_{CO} \cong 26$ STP cm^3 s^{-1} and $F_{N2} \cong 23$ STP cm^3 s^{-1}. The total pressure was maintained in the range P_T = 130−140 Torr with a partial pressure $P_{C6H5Br} \cong 1.5$ Torr of benzaldehyde determined from its IR absorption spectra. The efficiency of photolysis of C_6H_5Br is estimated to be ∼3% based on an absorption cross-section ∼4.9×10^{-19} cm^2 $molecule^{-1}$ (ref 23) and a laser fluence of ∼5.8×10^{16} photons cm^{-2} at 248 nm.

To obtain a desirable pressure of $C_6H_5C(O)CH_3$ and C_6H_5Br, the samples and the flow reactor were heated to 363 K with heated water circulated from a thermostatted bath through the jacket of the reactor. $C_6H_5C(O)CH_3$ (99%, Aldrich), C_6H_5Br (99%, Alfa Aesar), and N_2 (99.99%, Chiah Lung) were used without further purification. CO (99.999%, AGA Specialty Gases) was passed through a trap ∼ −55 °C before use.

The equilibrium geometry, vibrational wavenumbers and IR intensities of all species were calculated with B3LYP density-functional theory using the Gaussian09 program.[24] The B3LYP method uses Becke's three-parameter hybrid exchange functional with a correlation functional of Lee et al.[25,26] Dunning's correlation-consistent polarized-valence double-ζ basis set augmented with s, p, d, and f functions (aug-cc-pVDZ)[27,28] was applied in these calculations. For a chosen species, the rotational parameters of its ground and vibrationally excited (ν_i = 1) states were also calculated with B3LYP/aug-cc-pVDZ for spectral simulation. The anharmonic effects were calculated with a second-order perturbation approach using effective finite-difference evaluation of the third and semidiagonal fourth derivatives.

RESULTS

In this work, we used two sources of benzoyl radicals: irradiation of acetophenone, $C_6H_5C(O)CH_3$, at 248 nm[29] and irradiation of a mixture of bromobenzene, C_6H_5Br, and CO at 248 nm. Photolysis of C_6H_5Br at 248 nm produces C_6H_5 radicals[30] that react subsequently with CO to form C_6H_5CO

$$C_6H_5 + CO + M \rightarrow C_6H_5CO + M \quad (1)$$

with a rate coefficient of $k_1 = (2.2 \pm 0.8) \times 10^{-14}$ cm^3 $molecule^{-1}$ s^{-1} at 363 K.[31] Under our experimental conditions of P_T = 134 Torr and P_{CO} = 70.0 Torr, >90% C_6H_5CO is expected to be produced within 60 μs.

Transient Absorption Spectra Recorded upon Photolysis of $C_6H_5C(O)CH_3$ in N_2. Our previous work indicated that, upon irradiation of the precursor at low pressure, a fraction of the precursor became highly internally excited so that positive features appeared on each side of the downward parent band in the difference absorption spectrum.[20] These side lobes commonly interfere with nearby absorption bands of photodissociation products and hamper their detection. To avoid this interference, we employed excessive N_2 in the reactor as a quencher to thermalize photoirradiated $C_6H_5C(O)CH_3$ and other products in the system.

dx.doi.org/10.1021/jp2120934 | J. Phys. Chem. A 2012, 116, 6366−6374

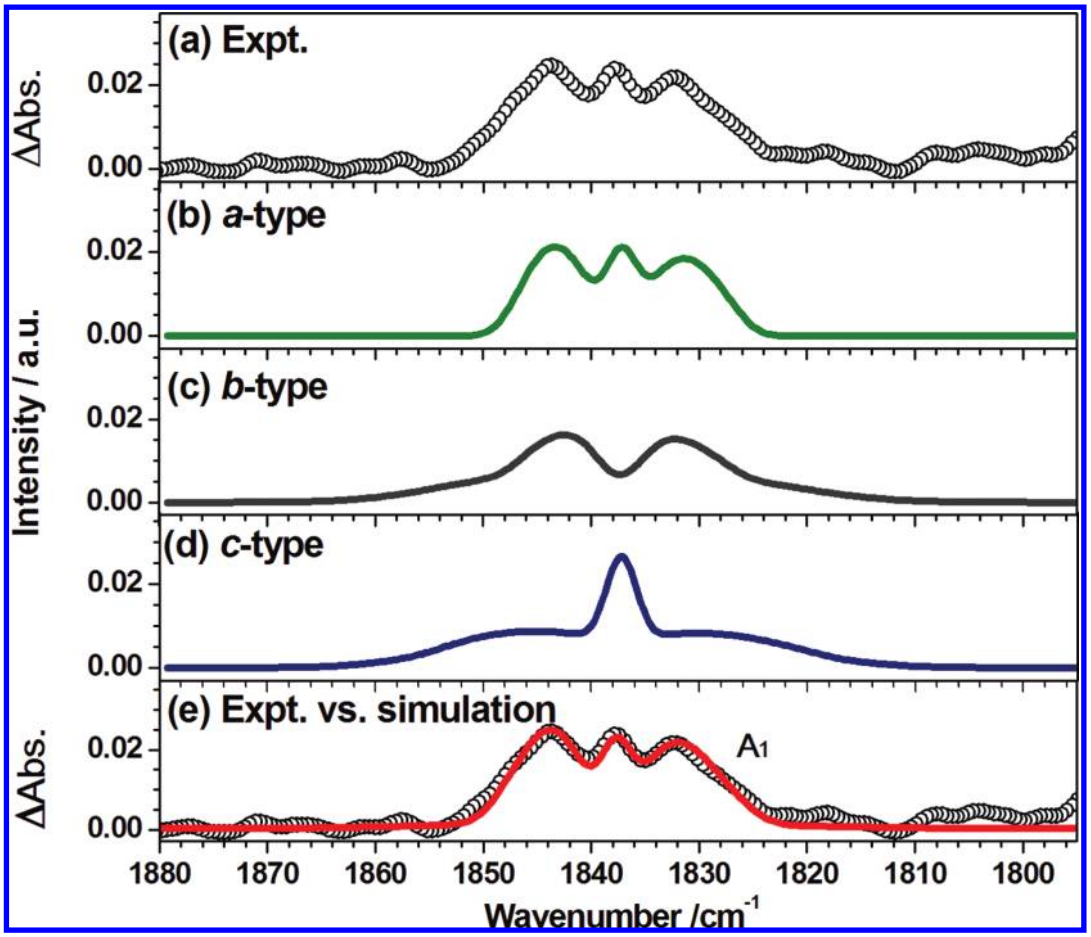

Figure 3. Comparison of simulated and observed spectra of the C═O stretching (ν_6) mode of C_6H_5CO. (a) Spectrum recorded at resolution 2 cm^{-1} and integrated for 5−40 μs after 248 nm laser irradiation of a flowing mixture of $C_6H_5Br/CO/N_2$ (1/47/46) at 363 K and 140 Torr. (b−d) *a*-type, *b*-type, and *c*-type components simulated with parameters are T = 363 K, J_{max} = 140, ν_0 = 1837.5 cm^{-1}, A'/A'' = 0.9993, B'/B'' = 0.9990, and C'/C'' = 0.9991. (e) Comparison of observed spectra (open circles) with the simulated spectrum (solid line) of C_6H_5CO with ν_0 = 1837.5 cm^{-1} and a hybrid *a*-/*b*-type band with a ratio of 0.84:0.16.

An absorption spectrum, at resolution 4 cm^{-1}, of a flowing mixture of $C_6H_5C(O)CH_3/N_2$ (1/213) at 107 Torr and 363 K in the region 1000−2200 cm^{-1} is shown in Figure 1a. The absorption of $C_6H_5C(O)CH_3$ is characterized by intense bands near 1708, 1366, and 1263 cm^{-1} and a few weaker ones at 3078, 2977, 2936, 1598, 1446, 1182, 1080, 1024, and 952 cm^{-1}, consistent with literature values.[32,33]

Representative differential spectra recorded at resolution 4 cm^{-1} upon irradiation of this flowing mixture at 248 nm and integrated at 20 μs intervals are shown in Figure 1b. The downward features near 1708, 1598, 1446, 1366, 1263, and 1182 cm^{-1} are due to loss of $C_6H_5C(O)CH_3$ upon irradiation. One intense feature near 1835 cm^{-1} and a weak one near 1130 cm^{-1}, labeled A_1 and A_2 in Figure 1b, respectively, appeared immediately after irradiation and decayed with time. Weak absorptions of CO near 2146 cm^{-1} were also observed. Because negative absorption of $C_6H_5C(O)CH_3$ might interfere with weak features, we corrected for this interference by adding back the portions due to depletion of $C_6H_5C(O)CH_3$ in such a way that the bands of $C_6H_5C(O)CH_3$ in the region 1280−1400 cm^{-1} became nearly flat. The resultant spectrum integrated for 0−10 μs, presented in Figure 1c, shows two additional weak bands near 1438 and 1590 cm^{-1}, marked with A_3 and A_4, respectively.

Transient Absorption Spectra Recorded upon Photolysis of $C_6H_5Br/CO/N_2$ Mixtures. To obtain additional evidence, we performed experiments using an alternative source of benzoyl radical. A gaseous mixture of $C_6H_5Br/CO/N_2$ (1/47/42, 134 Torr, 363 K) was subjected to laser irradiation at 248 nm; photolysis of C_6H_5Br at 248 nm produces C_6H_5 radicals that subsequently react with CO to form C_6H_5CO. Part of the absorption spectrum of this flowing mixture before irradiation is shown in Figure 2a; intense absorption bands 1585, 1480, 1072, and 1020 cm^{-1} and a few weaker ones near 1446 and 1002 cm^{-1} are due to C_6H_5Br. Representative temporally resolved difference spectra recorded at resolution 4 cm^{-1} and integrated at 20 μs intervals upon irradiation are presented in Figure 2b. For the period 0−20 μs upon photoirradiation, in addition to the downward features due to loss of C_6H_5Br, we observed two intense upward features near 1835 cm^{-1} and 1130 cm^{-1}; the positions and band shapes are identical to features A_1 and A_2 observed in experiments of $C_6H_5C(O)CH_3/N_2$ described in the preceding section. In these experiments, the absorption bands of C_6H_5Br near 1446 and 1585 cm^{-1} interfered with the weak A_3 and A_4 bands. We observed also a weak band near 1902 cm^{-1} marked D_1 in Figure 2b.

At a later period, as shown in Figure 2b for 20−40 μs, features A_1 and A_2 decreased in intensity, but bands in two

dx.doi.org/10.1021/jp2120934 | J. Phys. Chem. A 2012, 116, 6366−6374

additional sets appeared. The more intense bands near 1793, 1176, and 1195 cm^{-1} are marked B_1−B_3, and two weak features near 1687 and 1277 cm^{-1} are marked C_1 and C_2, respectively, in Figure 2b. These features increased in intensity at a later period, whereas features A_1 and A_2 decreased in intensity and nearly disappeared after 100 μs.

To obtain a more accurate rotational contour, we recorded also the transient spectra of the irradiated flowing mixture of $C_6H_5Br/CO/N_2$ (1/47/46, 140 Torr, 363 K) at resolution 2 cm^{-1}. For an acceptable ratio of signal-to-noise for the A_1 band near 1835 cm^{-1} at this resolution, we averaged data from 10 laser shots at each scan step and integrated spectra in the temporal range 5−40 μs; the resultant spectrum is shown in Figure 3a. In contrast to the rotational contour shown in Figures 1b and 2b, the PQR structure of this band is clearly recorded at this resolution. The increased noise due to higher resolution prevented us, however, from analyzing rotational contours of the A_2−A_4 bands at resolution 2 cm^{-1}.

Quantum-Chemical Calculations on C_6H_5CO. Geometries predicted with the B3LYP/aug-cc-pVDZ method for C_6H_5CO are shown in Figure S1 of the Supporting Information. Benzoyl radical is predicted to be planar with a C−C═O structure bent at angle 129.2°, consistent with the experimental result of 130°.[11]

The harmonic and anharmonic vibrational wavenumbers and IR intensities of C_6H_5CO predicted with the B3LYP/aug-cc-pVDZ method are listed in Table 1. The harmonic vibrational wavenumbers are nearly identical to those predicted with the UB3LYP/cc-pVTZ method reported previously.[15] One intense IR band of intensity ∼294 km mol^{-1} was predicted to be associated with the C═O stretching (ν_6) mode and has harmonic (anharmonic) vibrational wavenumbers 1879 (1838) cm^{-1}. The next intense band, with about one-fifth of the intensity of the former, is associated with the C−C stretching mode mixed with the C−H deformation mode (ν_{15}) and has harmonic (anharmonic) vibrational wavenumbers 1162 (1132) cm^{-1}. The third intense band, ν_{24} at 772 (723) cm^{-1} for the C−H out-of-plane deformation mode, is beyond the spectral region of our detection.

The predicted molecular axes, vibrational displacement vectors (thin arrows), and their corresponding dipole derivatives (thick dashed arrows) for the ν_6 and ν_{15} modes of C_6H_5CO are available in Figure S2 of the Supporting Information. The projection vector of the dipole derivative onto the molecular axes represents the weighting of the transition types. The C═O stretching (ν_6) band of C_6H_5CO is a hybrid type with a ratio of *a*-type/*b*-type = 84:16, whereas the C−C stretching/C−H deformation (ν_{15}) band has a ratio of *a*-type/*b*-type = 90:10. Rotational parameters *A*, *B*, and *C* calculated with the B3LYP/aug-cc-pVDZ method for the ground and the excited (ν_i = 1) states of these two vibrational modes of C_6H_5CO are listed in Table 2.

Absorption by the secondary product $C_6H_5C(O)Br$ might contribute to the observed spectrum. Harmonic vibrational wavenumbers and IR intensities predicted for this species using B3LYP/aug-cc-pVTZ are available in Table S1 of the Supporting Information.

DISCUSSION

Assignment of the A_1−A_4 Bands to C_6H_5CO. In the $C_6H_5C(O)CH_3/N_2$ system, $C_6H_5C(O)CH_3$ decomposes to mainly C_6H_5CO and CH_3 radicals upon irradiation at 248 nm.[29] Some C_6H_5CO might decompose further to C_6H_5 + CO.

Table 1. Comparison of Harmonic and Anharmonic Vibrational Wavenumbers/cm^{-1} and Relative IR Intensities (Listed in Parentheses) of C_6H_5CO Derived from Experiments and the B3LYP/aug-cc-pVDZ Calculation

mode[a]	harmonic[b]	anharmonic	matrix Ar[c]	gas[c]
ν_1	3197 (9)	3038		
ν_2	3193 (10)	3060		
ν_3	3185 (6)	3036		
ν_4	3178 (3)	3034		
ν_5	3168 (0)	3017		
ν_6	1879 (294)	1838	1824.4 (100)	1838 ± 1 (100)
ν_7	1631 (16)	1596	1594.8 (2)	1590 ± 10 (5)
ν_8	1615 (10)	1570	1581.0 (9)	
ν_9	1516 (0)	1490		
ν_{10}	1481 (12)	1459	1450.3 (4)	1438 ± 5 (8)
ν_{11}	1353 (5)	1334	1307.8 (<1)	
ν_{12}	1331 (6)	1315	1288.0 (1)	
ν_{13}	1202 (1)	1176		
ν_{14}	1185 (1)	1162		
ν_{15}	1162 (61)	1132	1136.2 (21)	1131 ± 3 (18)
ν_{16}	1101 (5)	1083	1070.4 (3)	
ν_{17}	1047 (3)	1026		
ν_{18}	1025 (0)	924		
ν_{19}	1021 (1)	1006		
ν_{20}	1007 (0)	947		
ν_{21}	964 (3)	912	935.8 (2)	
ν_{22}	872 (0)	828		
ν_{23}	807 (16)	790	789.7 (11)	
ν_{24}	772 (58)	723	755.9 (12)	
ν_{25}	699 (22)	659	687.8 (10)	
ν_{26}	636 (13)	624	624.7 (16)	
ν_{27}	623 (10)	614	610.4 (10)	
ref	this work	this work	15	this work

[a]Additional modes ν_{28}−ν_{33} are predicted to be 468 (2), 442 (0), 415 (0), 234 (0), 207 (3), and 100 (0) cm^{-1} for harmonic vibrations and 445, 433, 397, 223, 206, and 98 cm^{-1} for anharmonic vibrations. [b]The IR intensity for ν_6 is 294 km mol^{-1}. [c]Integrated IR intensities relative to ν_6 are listed in parentheses.

Table 2. Comparison of Rotational Parameters of C_6H_5CO in Their Ground and Vibrationally Excited States Predicted with the B3LYP/aug-cc-pVDZ Method

mode	*A* (cm^{-1})	*B* (cm^{-1})	*C* (cm^{-1})
ν_6 (1838 cm^{-1})	0.17835	0.05171	0.04009
ν_{15} (1132 cm^{-1})	0.17836	0.05167	0.04004
ground state	0.17849	0.05176	0.04013

In the $C_6H_5Br/CO/N_2$ system, C_6H_5Br decomposes to C_6H_5 + Br upon irradiation at 248 nm. The reaction of C_6H_5 with an excess of CO is not so rapid; under our experimental conditions, more than 90% of C_6H_5 is expected to react via reaction 1 to form C_6H_5CO within 60 μs. In addition to C_6H_5CO, possible products in this system include BrCO, $C_6H_5C(O)Br$, and $C_6H_5C(O)C_6H_5$. The common intermediates in these two systems are C_6H_5 and C_6H_5CO. C_6H_5 has no absorption near the 1800 cm^{-1} region that is typically associated with the C═O stretching mode, as we observed for feature A_1. Hence, the common transient features A_1−A_4 observed in both systems are most likely due to C_6H_5CO.

Consideration of Vibrational Wavenumbers. The IR spectrum of C_6H_5CO trapped in Ar matrix has been reported by Mardyukov and Sander[15] to have four most intense bands in

dx.doi.org/10.1021/jp2120934 | J. Phys. Chem. A 2012, 116, 6366−6374

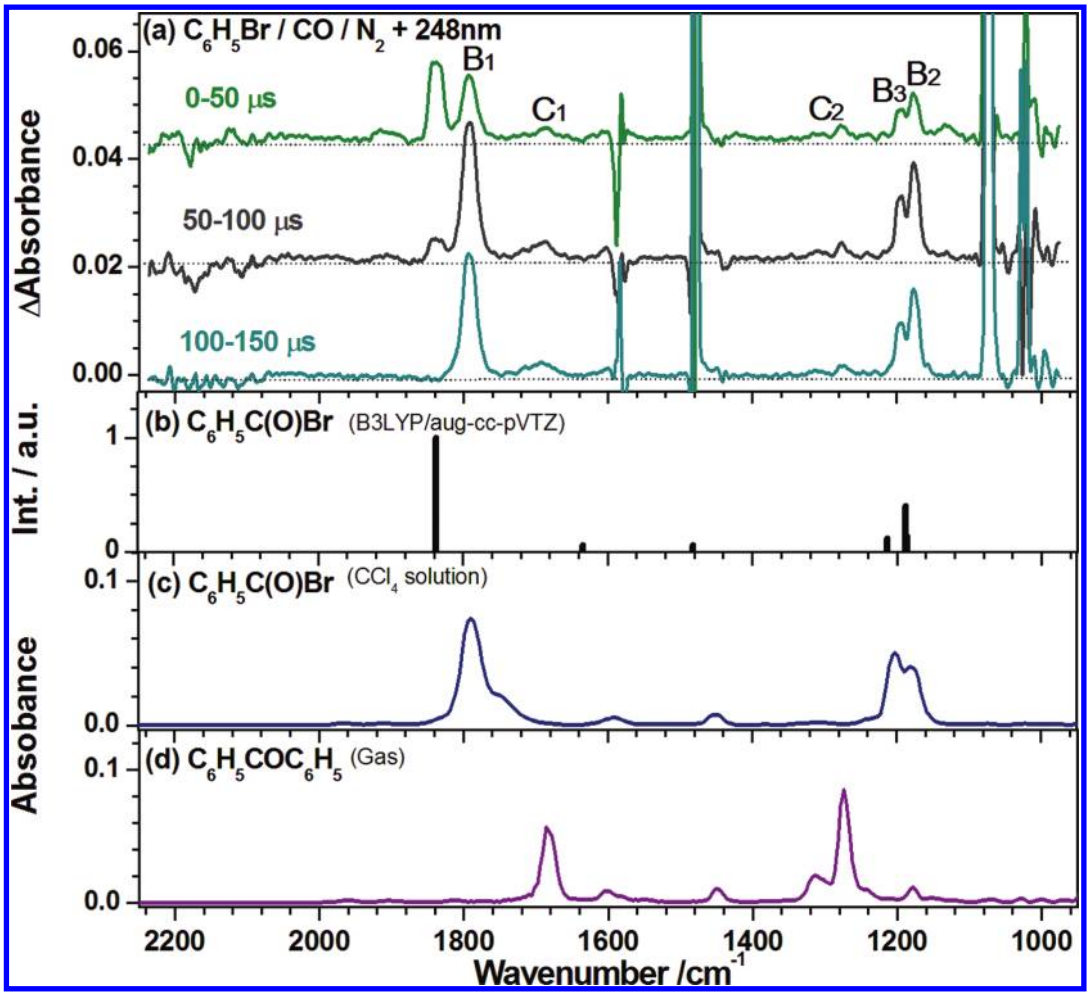

Figure 4. (a) Difference absorption spectra at 50 μs intervals upon laser photolysis at 248 nm (5 Hz, 46 mJ cm^{-2}) of a flowing mixture of C_6H_5Br/CO/N_2 (1/47/42) at 134 Torr and 363 K; resolution is 4 cm^{-1}. (b) Stick spectra of $C_6H_5C(O)Br$ according to harmonic vibrational wavenumbers and IR intensities predicted with the B3LYP/aug-cc-pVTZ method. (c) IR spectrum of $C_6H_5C(O)Br$ in a CCl_4 solution.[32] (d) Gaseous spectrum of $C_6H_5COC_6H_5$.[32]

our detection region at 1824.4, 1136.2, 1450.3, and 1581.0 cm^{-1}; other bands at 1594.8, 1288.0, and 1070.4 cm^{-1} are weaker. The new features with an intense band near 1835 (A_1), one weak feature near 1130 (A_2) and two extremely weak ones near 1438 (A_3) and 1590 cm^{-1} (A_4) observed in this work correspond well to the more intense absorption lines of C_6H_5CO isolated in solid Ar.

The B3LYP/aug-cc-pVDZ calculations predict four intense IR bands with harmonic (anharmonic) vibrational wavenumbers 1879 (1838), 1162 (1132), 1631 (1596), and 1481 (1459) cm^{-1} that are associated with the ν_6 (C═O stretching), ν_{15} (C−C stretching mixed with C−H deformation), ν_7 (in-phase $C_1C_2C_3/C_4C_5C_6$ antisymmetric stretching), and ν_{10} (out-of-phase $C_1C_2C_3/C_5C_6C_1$ symmetric stretching) modes of C_6H_5CO in the spectral region of our detection (Table 1). The deviations of predicted anharmonic vibrational wavenumbers from experimentally observed values are less than 1.4%. According to B3LYP/aug-cc-pVDZ, the relative IR intensities of these four bands are $A_1/A_2/A_3/A_4$ = 100:21:5:4, in satisfactory agreement with the experimentally observed ratio of 100:18:8:5 for features A_1−A_4. Hence, the most likely carrier for features A_1−A_4 is C_6H_5CO.

Rotational Contours. The rotational contour might provide further support for the identification. For comparison with observed spectra, we investigated the band contour for the C═O stretching (ν_6) and C−C stretching/C−H deformation (ν_{15}) modes of C_6H_5CO using molecular parameters predicted with the B3LYP/aug-cc-pVDZ method. With the SPECVIEW program,[34] we simulated the spectrum of each band using predicted rotational parameters A′, A″, B′, B″, C′, C″, J_{max} = 140, ΔK_{max} = 11, T = 363 K, and a width (full width at half-maximum) of 2 cm^{-1}.

A comparison of the simulated and observed transient spectra recorded at resolution 2 cm^{-1} and integrated for period 5−40 μs upon photolysis is shown in Figure 3 for the region 1795−1880 cm^{-1}. The *a*-, *b*-, and *c*-type bands simulated for the C═O stretching (ν_6) mode of C_6H_5CO according to quantum-chemically predicted parameters are shown in traces b−d of Figure 3, respectively. The resultant spectrum based on the *a*-type/*b*-type ratio of 84:16 predicted according to the vector of associated dipole derivatives is shown as red thick lines in Figure 3e and compared with the experimentally observed spectrum of feature A_1 shown as open circles. The observed rotational contour agrees satisfactorily with predicted contours when we used ν_0 = 1837.5 cm^{-1}. The harmonic (anharmonic) vibrational wavenumbers of 1879 (1838) cm^{-1} predicted for C_6H_5CO are consistent with this fit.

dx.doi.org/10.1021/jp2120934 | J. Phys. Chem. A 2012, 116, 6366−6374

Similarly, the simulated spectra for the C−C stretching/C−H deformation (ν_{15}) mode of C_6H_5CO fit with the experimentally observed spectrum of feature A_2 when we used ν_0 = 1131 cm^{-1} for C_6H_5CO. The harmonic (anharmonic) vibrational wavenumbers of 1162 (1132) cm^{-1} predicted for C_6H_5CO agree satisfactorily with the fitted value. The weak feature A_3 was fitted to be 1438 cm^{-1}. Considering the fitting errors and the spectral resolution, we estimate errors for the wavenumbers of the intense features A_1 as ±1 cm^{-1}, and those for A_2 and A_3 as ±3 and ±5 cm^{-1}, respectively. The A_4 band near 1590 cm^{-1} is too weak to fit, and the estimated uncertainty is ∼10 cm^{-1}.

In summary, after comparison of observed vibrational wavenumbers, relative IR intensities and rotational contours with those predicted with quantum-chemical calculations, we assigned observed features A_1−A_4 to C_6H_5CO. The observation of one intense band at 1838 ± 1 cm^{-1}, one weak band near 1131 ± 3, and two extremely weak bands near 1438 ± 5 and 1590 ± 10 cm^{-1} of gaseous C_6H_5CO closely resembles the absorption lines at 1824.4, 1136.2, 1450.3, and 1594.8/1581.0 cm^{-1} observed for C_6H_5CO in solid Ar (Table 1).[15] For comparison, the C═O stretching mode at 1838 cm^{-1} for C_6H_5CO is slightly larger than the corresponding value 1830 cm^{-1} of $C_6H_5C(O)OO$ reported previously,[19] as the C−OO bonding is expected to decrease the C═O bonding in $C_6H_5C(O)OO$.

Assignment of Features B_1−B_3 to $C_6H_5C(O)Br$. In photolysis experiments of $C_6H_5Br/CO/N_2$, the intensities of features B_1−B_3 gradually increased, whereas those of features A_1 and A_2 decreased. Features B_1−B_3 were unobserved in photolysis of $C_6H_5C(O)CH_3$. Hence, the most likely carrier of features B_1−B_3 is the reaction product of C_6H_5CO with Br or CO, the species that exist only in experiments with $C_6H_5Br/CO/N_2$ but not in experiments with $C_6H_5C(O)CH_3/N_2$. A reaction between C_6H_5CO and CO is unlikely to occur, whereas a reaction between C_6H_5CO and Br to form stable compound $C_6H_5C(O)Br$ is feasible.

Figure 4 compares features observed at 0−50, 50−100, and 100−150 μs, shown in panel a, with the stick spectrum predicted for $C_6H_5C(O)Br$ with the B3LYP/aug-cc-pVTZ method shown in panel b and the literature spectrum of $C_6H_5C(O)Br$ in a CCl_4 solution.[32] The observed vibrational wavenumbers of features B_1−B_3 near 1793, 1176, and 1195 cm^{-1} match satisfactorily values 1776, 1170, and 1192 cm^{-1} reported for $C_6H_5C(O)Br$ in CCl_4 and the harmonic vibrational wavenumbers of 1837, 1214, and 1188/1186 cm^{-1} predicted with the B3LYP/aug-cc-pVTZ method. Hence, we assign features B_1−B_3 to absorption bands of $C_6H_5C(O)Br$; the B_1 features is associated with the C═O stretching (ν_6) mode.

Possible Assignments for Features C_1, C_2, and D_1. In photolysis experiments of $C_6H_5Br/CO/N_2$, weak features C_1 and C_2 near 1687 and 1277 cm^{-1} appeared at later stages of the experiments but were unobserved after photolysis of $C_6H_5C(O)CH_3$. The small intensities of these features preclude definitive assignment, but these features are likely due to absorption of $C_6H_5C(O)C_6H_5$ of which a spectrum in the gaseous phase is shown in Figure 4d for comparison.[32] The wavenumbers of band maxima near 1682 and 1274 cm^{-1} agree satisfactorily with our observation.

The production of $C_6H_5C(O)C_6H_5$ might be rationalized from the reaction of C_6H_5CO with C_6H_5; both species were present in the system. The small intensity indicates that most C_6H_5 reacted with CO rapidly to form C_6H_5CO, which further reacted rapidly with Br to form $C_6H_5C(O)Br$, and only a small fraction of C_6H_5 and C_6H_5CO has a chance to react with each other. One would expect that these features might also appear in photolysis experiments of $C_6H_5C(O)CH_3$, if some energetic C_6H_5CO further decomposed to C_6H_5 and CO or some C_6H_5 was produced directly from photolysis. These two features C_1 and C_2 near 1687 and 1277 cm^{-1} are, however, overlapped with intense bands of $C_6H_5C(O)CH_3$ near 1708 and 1263 cm^{-1} shown in Figure 1a; the intense negative features of $C_6H_5C(O)CH_3$ upon photolysis prevent the observation of features C_1 and C_2.

A weak feature D_1 near 1902 cm^{-1} was observed along with features A_1 and A_2 in experiments with $C_6H_5Br/CO/N_2$ at the early stages after irradiation. Although we are unable to provide a definitive assignment for this feature because of its small intensity, we think that the most likely carrier of this band is BrCO because upon photolysis both C_6H_5 and Br were produced. Similar to the observation of C_6H_5CO due to reaction of C_6H_5 + CO, the product BrCO is expected to be produced from Br + CO. No IR spectrum of BrCO has been reported. A similar compound, ClCO, was reported to have an absorption band at 1884.6 cm^{-1}.[35] Because the bonding between Br and CO is weaker than that between Cl and CO, one would expect that the C═O stretching wavenumber of BrCO to be slightly greater than that of ClCO, consistent with our experimental observation. Quantum-chemical calculations using B3LYP/aug-cc-pVTZ predicted harmonic vibrational wavenumbers to be ν_1 = 1944 cm^{-1} for ClCO (ref 35) and 2028 cm^{-1} for BrCO, in satisfactory agreement with the observed band at 1885 cm^{-1} for ClCO and the feature D_1 near 1902 cm^{-1} tentatively assigned to BrCO.

Reaction Kinetics. The experimental setup is intended for spectral study rather than kinetic study because the photolysis beam path is quite different from the IR absorption beam path and only a small fraction (∼4%) of gases in the reactor was photolyzed. We are unable to determine the absolute concentration of C_6H_5, C_6H_5CO, and $C_6H_5C(O)Br$ because we do not know their IR absorption cross-sections. Nevertheless, we try to obtain some information on the reaction kinetics according to the observed temporal profiles so that we can understand if observed kinetics are reasonable.

As shown in Figure 2, features A_1 and A_2 of C_6H_5CO appeared promptly, decreased in intensity, and became nearly unobservable 100 μs after photolysis of the $C_6H_5Br/CO/N_2$ mixture, whereas features B_1−B_3 of $C_6H_5C(O)Br$ increased in intensity with time. The temporal profiles of the relative concentration of C_6H_5CO, integrated over the spectral range 1816−1858 cm^{-1} of feature A_1, and of the relative concentration of $C_6H_5C(O)Br$, integrated over the spectral range 1771−1812 cm^{-1} of feature B_1, are shown in Figure 5.

Following photolysis of C_6H_5Br to form C_6H_5 and Br, the reaction mechanism is expected to be

$$C_6H_5 + CO + M \rightarrow C_6H_5CO + M \quad (1)$$

$$Br + CO + M \rightarrow BrCO + M \quad (2)$$

$$C_6H_5CO + Br + M \rightarrow C_6H_5C(O)Br + M \quad (3)$$

$$C_6H_5 + Br + M \rightarrow C_6H_5Br + M \quad (4)$$

$$C_6H_5CO + C_6H_5 + M \rightarrow C_6H_5C(O)C_6H_5 + M \quad (5)$$

The rise of C_6H_5CO, reaction 1, is expected to be pseudofirst-order because [CO] = 1.86 × 10^{18} molecules

dx.doi.org/10.1021/jp2120934 | J. Phys. Chem. A 2012, 116, 6366−6374

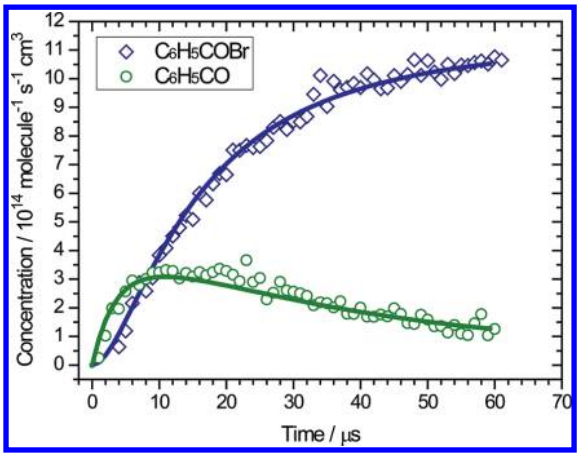

Figure 5. Plot of intensities of the ν_6 band of C_6H_5CO integrated over 1816−1858 cm^{-1} and the ν_6 band of $C_6H_5C(O)Br$ integrated over 1771−1812 cm^{-1} upon photolysis at 248 nm of a flowing mixture of $C_6H_5Br/CO/N_2$ (1/47/42) at 134 Torr and 363 K as a function of the reaction duration. Simulated results in the region of 0−60 μs are shown with solid lines; see text.

cm^{-3}. The loss of C_6H_5CO is expected to be due mainly to reaction 3 because the concentration of C_6H_5 in reaction 5 is expected to be small. Hence, we use a simplified mechanism comprising reactions 1−3 to describe the rise and fall of C_6H_5CO and the formation of $C_6H_5C(O)Br$.

The rate coefficient of reaction 1 was reported to be $k_1 = (1.41 \pm 0.47) \times 10^{-12} \exp[-(1507 \pm 109)/T]$ cm^3 $molecule^{-1}$ s^{-1} for P = 12−120 Torr and T = 295−500 K; $k_1 = (2.2 \pm 0.8) \times 10^{-14}$ cm^3 $molecule^{-1}$ s^{-1} at 363 K.[31] The rate coefficient of reaction 2 is unreported. The rate coefficient of the similar reaction Cl + CO + M was recommended to be $1.33 \times 10^{-33} (T/298)^{-3.80}$ cm^6 $molecule^{-2}$ s^{-1};[36] at 363 K and 134 Torr, the bimolecular rate coefficient is 2.3×10^{-15} cm^3 $molecule^{-1}$ s^{-1}. This value is about one tenth of k_1, indicating that reaction 2 is likely unimportant relative to reaction 1.

Analytical solution of the differential equations involving even only reactions 1 and 3 is unattainable because [Br], with $[Br]_0 = [C_6H_5]_0$, might not be large enough to warrant the pseudofirst-order conditions for reaction 3, especially at the later stages. An accurate kinetic simulation on the concentrations of C_6H_5CO and $C_6H_5C(O)Br$ according to reactions 1 and 3 is also difficult because $[Br]_0$ and $[C_6H_5]_0$ could not be accurately determined. We could only estimate $[Br]_0$ and $[C_6H_5]_0$ according to the absorption cross-section $\sim 4.9 \times 10^{-19}$ cm^2 $molecule^{-1}$ determined for C_6H_5Br at 248 nm (ref 23) and a laser fluence 5.8×10^{16} photons cm^{-2} and derived the initial concentrations $[Br]_0 = [C_6H_5]_0 \cong 1.24 \times 10^{15}$ molecules cm^{-3} in the photolyzed volume and used these concentrations in the simulation by assuming slow diffusion within 100 μs under our experimental conditions. Because the absolute concentrations of C_6H_5CO and $C_6H_5C(O)Br$ are unattainable, we could only compare the general shape of the simulated temporal profiles with the observed temporal profiles; the observed temporal profiles of integrated intensities of C_6H_5CO and $C_6H_5C(O)Br$ were scaled to provide the best fits. The best simulation, derived from $k_1 = (4.6 \pm 1.4) \times 10^{-14}$ cm^3 $molecule^{-1}$ s^{-1} and $k_3 = (1.6 \pm 0.5) \times 10^{-10}$ cm^3 $molecule^{-1}$ s^{-1}, is shown as solid curves in Figure 5; the error limits represent only fitting uncertainties. The scaling factors used for observed concentrations imply that the quantum-chemically predicted value of 294 km mol^{-1} is about 20% smaller than the IR intensity that we employed in the fitting of C_6H_5CO, whereas the predicted value of 334 km mol^{-1} for $C_6H_5C(O)Br$ is about 55% greater than that employed in the fitting. These deviations are within expected errors for IR intensities predicted with quantum-chemical calculations.

Because the concentration of CO is known, the fitted value of k_1 is more reliable than k_3. The $k_1 = (4.6 \pm 1.4) \times 10^{-14}$ cm^3 $molecule^{-1}$ s^{-1} at 363 K estimated from the simulation is about twice the only literature value, $k_1 = (2.2 \pm 0.8) \times 10^{-14}$ cm^3 $molecule^{-1}$ s^{-1}.[31] Further studies are needed in order to understand this discrepancy. The fitted value of k_3 depends on $[Br]_0$, which could be estimated only from photolysis yield; the value of $k_3 = (1.6 \pm 0.5) \times 10^{-10}$ cm^3 $molecule^{-1}$ s^{-1} should hence be considered as a rough estimate of the previously unreported rate coefficient. That is to say, reaction 3 proceeds nearly at the collision rate. This estimate is consistent with the reported rate coefficient of the reaction

$$C_6H_5CO + H + M \rightarrow C_6H_5C(O)H + M \qquad (6)$$

in which $k_6 = (5.0 \pm 1.6) \times 10^{-11}$ cm^3 $molecule^{-1}$ s^{-1} at 298 K and 0.75 Torr.[37]

CONCLUSIONS

IR absorption bands near 1838, 1131, 1438, and 1590 cm^{-1} were observed with a step-scan Fourier-transform spectrometer upon irradiation at 248 nm of a gaseous flowing mixture of $C_6H_5C(O)CH_3$ in N_2, and a mixture of $C_6H_5Br/CO/N_2$. On considering possible chemical reactions and comparing vibrational wavenumbers, relative IR intensities, and rotational contours observed experimentally and predicted with quantum-chemical calculations, we attributed the intense absorption bands near 1838 ± 1 cm^{-1} to the C═O stretching (ν_6) mode, the weak band near 1131 ± 3 cm^{-1} to the C−C stretching/C−H deformation (ν_{15}) mode, and the extremely weak bands near 1438 ± 5 and 1590 ± 10 cm^{-1} to the out-of-phase $C_1C_2C_3/C_5C_6C_1$ symmetric stretching (ν_{10}) and in-phase $C_1C_2C_3/C_4C_5C_6$ antisymmetric stretching (ν_7) modes of C_6H_5CO, respectively.

In experiments of $C_6H_5Br/CO/N_2$, intense IR absorption bands near 1793, 1176, and 1195 cm^{-1} were observed at a later stage of reaction and are assigned to $C_6H_5C(O)Br$, produced from reaction of C_6H_5CO with Br. Weak bands near 1687 and 1277 cm^{-1} observed at a later stage of reaction might be assigned to $C_6H_5C(O)C_6H_5$, produced from reaction of C_6H_5CO with C_6H_5. A weak band produced at the early stage of reaction near 1902 cm^{-1} might be assigned to the C═O stretching mode of BrCO. Simulation of the observed temporal profiles of C_6H_5CO and $C_6H_5C(O)Br$ yield $k_1 \cong (4.6 \pm 1.4) \times 10^{-14}$ cm^3 $molecule^{-1}$ s^{-1} and k_3 on the order of 10^{-10} cm^3 $molecule^{-1}$ s^{-1} at 363 K.

ASSOCIATED CONTENT

Supporting Information

Additional information on the geometries predicted with the B3LYP/aug-cc-pVDZ method for C_6H_5CO (Figure S1), the predicted molecular axes, vibrational displacement vectors, and their corresponding dipole derivatives for the ν_6 and ν_{15} modes of C_6H_5CO (Figure S2), and harmonic vibrational wavenumbers and IR intensities predicted for $C_6H_5C(O)Br$ using the B3LYP/aug-cc-pVTZ method (Table S1). This material is available free of charge via the Internet at http://pubs.acs.org.

dx.doi.org/10.1021/jp2120934 | J. Phys. Chem. A 2012, 116, 6366−6374

AUTHOR INFORMATION

Corresponding Author

*Fax: +886-3-5713491. E-mail: yplee@mail.nctu.edu.tw.

Notes

The authors declare no competing financial interest.

ACKNOWLEDGMENTS

National Science Council of Taiwan (Grant No. NSC100-2745-M-009-001-ASP) and Ministry of Education of Taiwan ("Aim for the Top University Plan" of National Chiao Tung University) supported this work. The National Center for High-Performance Computing provided computer time. We thank V. Stakhursky and T. A. Miller for providing the SpecView software for spectral simulation.

REFERENCES

(1) Allen, N. S.; Marin, M. C.; Edge, M.; Davies, D. W.; Garret, J.; Jones, F.; Navaratnam, S.; Parsons, B. J. *J. Photochem. Photobiol., A* **1999**, *126*, 135−149.
(2) Calvert, J. G.; Atkinson, R.; Becker, K. H.; Kamens, R. M.; Seinfeld, J. H.; Wallington, T. J.; Yarwood, G. *The Mechanisms of Atmospheric Oxidation of Aromatic Hydrocarbons*; Oxford University Press: London, U.K., 2002.
(3) Atkinson, R. *Atmos. Environ.* **2000**, *34*, 2063−2101.
(4) McDade, C. E.; Lenhardt, T. M.; Bayes, K. D. *J. Photochem.* **1982**, *20*, 1−7.
(5) Heuss, J. M.; Glasson, W. A. *Environ. Sci. Technol.* **1968**, *2*, 1109−1116.
(6) Atkinson, R.; Lloyd, A. C. *J. Phys. Chem. Ref. Data* **1984**, *13*, 315−444.
(7) Fahr, A.; Mallard, S. G.; Stein, S. E. *Twenty-First Symposium (International) on Combustion*; The Combustion Institute: Pittsburgh, PA, 1986; pp 825−831.
(8) Kolczak, U.; Rist, G.; Dietliker, K.; Wirz, J. *J. Am. Chem. Soc.* **1996**, *118*, 6477−6489.
(9) Jockusch, S.; Koptyug, I. V.; McGarry, P. F.; Sluggett, G. W.; Turro, N. J.; Watkins, D. M. *J. Am. Chem. Soc.* **1997**, *119*, 11495−11501.
(10) Huggenberger, C.; Lipscher, J.; Fischer, H. *J. Phys. Chem.* **1980**, *84*, 3467−3474.
(11) Bennett, J. E.; Mile, B. *Trans. Faraday Soc.* **1971**, *67*, 1587−1597.
(12) Merzlikine, A. G.; Voskresensky, S. V.; Danilov, E. O.; Neckers, D. C.; Fedorov, A. V. *Photochem. Photobiol. Sci.* **2007**, *6*, 608−613.
(13) Colley, C. S.; Grills, D. C.; Besley, N. A.; Jockusch, S.; Matousek, P.; Parker, A. W.; Towrie, M.; Turro, N. J.; Gill, P. M. W.; George, M. W. *J. Am. Chem. Soc.* **2002**, *124*, 14952−14958.
(14) Kolano, C.; Bucher, G.; Wenk, H. H.; Jaeger, M.; Schade, O.; Sander, W. *J. Phys. Org. Chem.* **2004**, *17*, 207−214.
(15) Mardyukov, A.; Sander, W. *Eur. J. Org. Chem.* **2010**, *15*, 2904−2909.
(16) Chen, S.-Y.; Lee, Y.-P. *J. Chem. Phys.* **2010**, *132*, 114303−114313.
(17) Chu, L.-K.; Lee, Y.-P. *J. Chem. Phys.* **2010**, *133*, 184303−184313.
(18) Chen, J.-D.; Lee, Y.-P. *J. Chem. Phys.* **2010**, *134*, 094304−094315.
(19) Golec, B.; Chen, J.-D.; Lee, Y.-P. *J. Chem. Phys.* **2011**, *135*, 224302−224311.
(20) Chu, L.-K.; Lee, Y.-P.; Jiang, E.-Y. *J. Chem. Phys.* **2004**, *120*, 3179−3184.
(21) Uhmann, W.; Becker, A.; Taran, C.; Siebert, F. *Appl. Spectrosc.* **1991**, *45*, 390−397.
(22) Clark, L. B.; Tinoco, I., Jr. *J. Am. Chem. Soc.* **1965**, *87*, 11−15.
(23) Rasmusson, M.; Lindh, R.; Lascoux, N.; Tarnovsky, A. N.; Kadi, M.; Kühn, O.; Sundström, V.; Åkesson, E. *Chem. Phys. Lett.* **2003**, *367*, 759−766.
(24) Frisch, M. J.; Trucks, G. W.; Schlegel, H. B.; Scuseria, G. E.; Robb, M. A.; Cheeseman, J. R.; Scalmani, G.; Barone, V.; Mennucci, B.; Petersson, G. A.; Nakatsuji, H.; Caricato, M.; Li, X.; Hratchian, H. P.; Izmaylov, A. F.; Bloino, J.; Zheng, G.; Sonnenberg, J. L.; Hada, M.; Ehara, M.; Toyota, K.; Fukuda, R.; Hasegawa, J.; Ishida, M.; Nakajima, T.; Honda, Y.; Kitao, O.; Nakai, H.; Vreven, T.; Montgomery, J. A., Jr.; Peralta, J. E.; Ogliaro, F.; Bearpark, M.; Heyd, J. J.; Brothers, E.; Kudin, K. N.; Staroverov, V. N.; Kobayashi, R.; Normand, J.; Raghavachari, K.; Rendell, A.; Burant, J. C.; Iyengar, S. S.; Tomasi, J.; Cossi, M.; Rega, N.; Millam, J. M.; Klene, M.; Knox, J. E.; Cross, J. B.; Bakken, V.; Adamo, C.; Jaramillo, J.; Gomperts, R.; Stratmann, R. E.; Yazyev, O.; Austin, A. J.; Cammi, R.; Pomelli, C.; Ochterski, J. W.; Martin, R. L.; Morokuma, K.; Zakrzewski, V. G.; Voth, G. A.; Salvador, P.; Dannenberg, J. J.; Dapprich, S.; Daniels, A. D.; Farkas, O.; Foresman, J. B.; Ortiz, J. V.; Cioslowski, J.; Fox, D. J. *Gaussian 09*, revision A.02; Gaussian, Inc.: Wallingford, CT, 2009.
(25) Becke, A. D. *J. Chem. Phys.* **1993**, *98*, 5648−5652.
(26) Lee, C.; Yang, W.; Parr, R. G. *Phys. Rev. B* **1988**, *37*, 785−789.
(27) Dunning, T. H., Jr. *J. Chem. Phys.* **1989**, *90*, 1007−1023.
(28) Woon, D. E.; Dunning, T. H., Jr. *J. Chem. Phys.* **1993**, *98*, 1358−1371.
(29) Zhao, H.-Q.; Cheung, Y.-S.; Liao, C.-L.; Liao, C. X.; Ng, C.-Y.; Li, W.-K. *J. Chem. Phys.* **1997**, *107*, 7230−7241.
(30) Kadi, M.; Davidsson, J.; Tarnovsky, A. N.; Rasmusson, M.; Åkesson, E. *Chem. Phys. Lett.* **2001**, *350*, 93−98.
(31) Nam, G. J.; Xia, W.; Park, J.; Lin, M. C. *J. Phys. Chem. A* **2000**, *104*, 1233−1239.
(32) Stein, S. E. Infrared Spectra. In *NIST Chemistry WebBook*, NIST Standard Reference Database Number 69; Linstrom, P. J., Mallard, W. G., Eds.; National Institute of Standards and Technology: Gaithersburg, MD, 2003; p 20899 (see http://webbook.nist.gov).
(33) Gambi, A.; Giorgianni, S.; Passerini, A.; Visinoni, R.; Ghersetti, S. *Spectrochim. Acta* **1980**, *36A*, 871−878.
(34) Stakhursky, V.; Miller, T. A.SPECVIEW: Simulation and Fitting of Rotational Structure of Electronic and Vibronic Bands. Presented at 56th OSU International Symposium on Molecular Spectroscopy, Columbus, OH, 2001; http://www.chemistry.ohio-state.edu/~vstakhur.
(35) Chen, S.-H.; Chu, L.-K.; Chen, Y.-J.; Chen, I.-C.; Lee, Y.-P. *Chem. Phys. Lett.* **2001**, *333*, 365−370.
(36) Atkinson, R.; Baulch, D. L.; Cox, R. A.; Crowley, J. N.; Hampson, R. F.; Hynes, R. G.; Jenkin, M. E.; Rossi, M. J.; Troe, J. *Atmos. Chem. Phys.* **2007**, *7*, 981−1191.
(37) Buth, R.; Hoyermann, K.; Rohde, G. *Twenty-Fourth Symposium (International) on Combustion*; The Combustion Institute: Pittsburgh, PA, 1992; pp 669−674.

NOTE ADDED AFTER ASAP PUBLICATION

This paper was published ASAP on March 15, 2012. Changes were made to Tables 1 and 2 and associated text in the Results and Discussion sections. The corrected version was reposted on April 26, 2012.